ChemPhysChem

Research Article
doi.org/10.1002/cphc.202200589

Chemistry Europe
European Chemical Societies Publishing

www.chemphyschem.org

Orange Peel Biomass-derived Carbon Supported Cu Electrocatalysts Active in the CO_2-Reduction to Formic Acid

Tanvir Miah,[a] Palmarita Demoro,[b] Izuchika Nduka,[a] Federica De Luca,[b] Salvatore Abate,[b] and Rosa Arrigo*[a]

We report a green, wet chemistry approach towards the production of C-supported Cu electrocatalysts active in the CO_2 reduction to formic acid. We use citrus peels as a C support precursor and as a source of reducing agents for the Cu cations. We show that orange peel is a suitable starting material compared to lemon peel for the one-pot hydrothermal synthesis of Cu nanostructures affording better Cu dispersion as well as productivity and selectivity towards formic acid. We rationalize this finding in terms of the beneficial chemical composition of the orange peel, which favors both the reduction of the Cu precursor as well as the carbon matrix. This work demonstrates new viable opportunities for the reuse of citrus waste on a rational basis.

Introduction

The use of carbonaceous materials in sustainable energy applications is extensively explored, including catalysis,[1] electrocatalysis[2] and reversible batteries technologies.[3] Especially in energy storage and conversion, large production of carbon will be required for the widespread use of such new technologies. In the context of a circular economy, the production of C materials from biomass waste[4] generates opportunities to increase the economic value of the waste, which in turn open up pathways for new markets.[5] For example, Tiwari et al. have recently reported on the development of multi-heteroatom-doped carbon electrocatalysts from waste-yeast biomass for water splitting.[6] Other uses include the conversion of various biomasses in value added chemicals such as levulinic acid.[7] Herein, we are concerned with the valorisation of citrus waste. In 2019, the global citrus extract market size was valued at 5.6 billion USD with an expected annual growth rate of 4.2% from 2020 to 2027.[8] It is expected that citrus waste will also grow proportionally to the 50–60% of the global volume of citrus processed.[5] On the one hand, the disposal of citrus waste requires appropriate management due to the potential negative effects of its chemical constituents (organic matter, oils and free acids) on the environment. On the other hand, citrus waste constituents include chemical compounds of added value (e.g. phenolic and flavonoids, essential oils, pectin and other fibres) which have motivated much research into their extraction.[9] Amongst the chemical compounds contained in citrus peel, ascorbic acid is currently used as both reducing agent and capping agents in the synthesis of Cu nanoparticles active in CO_2 electroreduction.[10] This study aims at demonstrating the viability of the direct utilization of the citrus waste in a one-pot synthesis of C-supported Cu nanoparticles using C precursors naturally enriched with ascorbic acid. Thus, the direct utilization of the citrus peel is two-fold advantageous: i) it provides the carbon support for the nanoparticles; ii) it provides the ascorbic acid needed for Cu reduction with no need to extract it from natural sources and to add it as reducing agent in the synthesis. In order to explore this idea, we use here two commercial citrus peels, specifically lemon and orange peels. The morphological characterization of the samples by electron microscopy and the chemical speciation by means of X-ray photoelectron spectroscopy will be presented together with the reactivity data in CO_2 electroreduction with the goal to identify direction for viable utilization of biomass in the preparation of materials for energy application. We will show that the chemical nature of the biomass will influence not only the chemical speciation of the as prepared electrocatalyst, but also its behavior and stability under reaction conditions. This contribution demonstrates that the utilization of biomass is application-dependent and requires a rational approach for effective utilisation.

Results and Discussion

The samples obtained via the synthetic procedure described in the experimental section are herein referred to as Cu–L and Cu–O, where L stands for lemon peel and O for orange peel, respectively.

X-ray fluorescence analysis of the samples reveals a bulk chemical composition of metals expressed in weight percent

[a] T. Miah, I. Nduka, Dr. R. Arrigo
School of Science, Engineering and Environment
University of Salford
M5 4WT, Manchester, UK
E-mail: r.arrigo@salford.ac.uk
[b] P. Demoro, F. De Luca, Dr. S. Abate
ERIC aisbl and CASPE/INSTM, Dpt. ChiBioFarAM
University of Messina
Viale F. Stagno D'Alcontres 31, Messina, 98166, Italy

Supporting information for this article is available on the WWW under https://doi.org/10.1002/cphc.202200589

as follows: Cu–O: 18.4% Cu, 1.2% Ca, 0.5% K and 4.2% S; Cu–L: 14.1% Cu, 1.2% Ca, 0.7% K and 3.6% S.

The scanning electron micrographs (SEM) in secondary electron (SE) mode in Figure 1a–c for Cu–O measured at increasing magnification show the morphology of the sample characterized by a highly porous support homogeneously decorated with round Cu nanoparticles ranging between 270 nm and 525 nm in size (average particle size determined by statistical analysis on the SEM images is 370 ± 60 nm). The micrograph in back-scattered electron (BSE) mode in Figure 1d enables us to identify more precisely the metal nanoparticles (brighter area are due to the heavier element, in this case Cu) and reveals that the particles are indeed covered by an overlayer, probably carbonaceous in nature. A few large agglomerated crystals of a S, O, Cu containing phase are also observed in the low magnification images (Figure S1 in the Supporting Information). In contrast, the Cu–L sample is characterized mainly by unsupported large single crystals (for example the one at the top left corner in Figure 1e) or deposited crystals of a not well-defined morphology (Figure 1f–h). The EDX analysis of such a large single crystal in Cu–L (Figure S1) is consistent with a S–O-containing Cu phase.

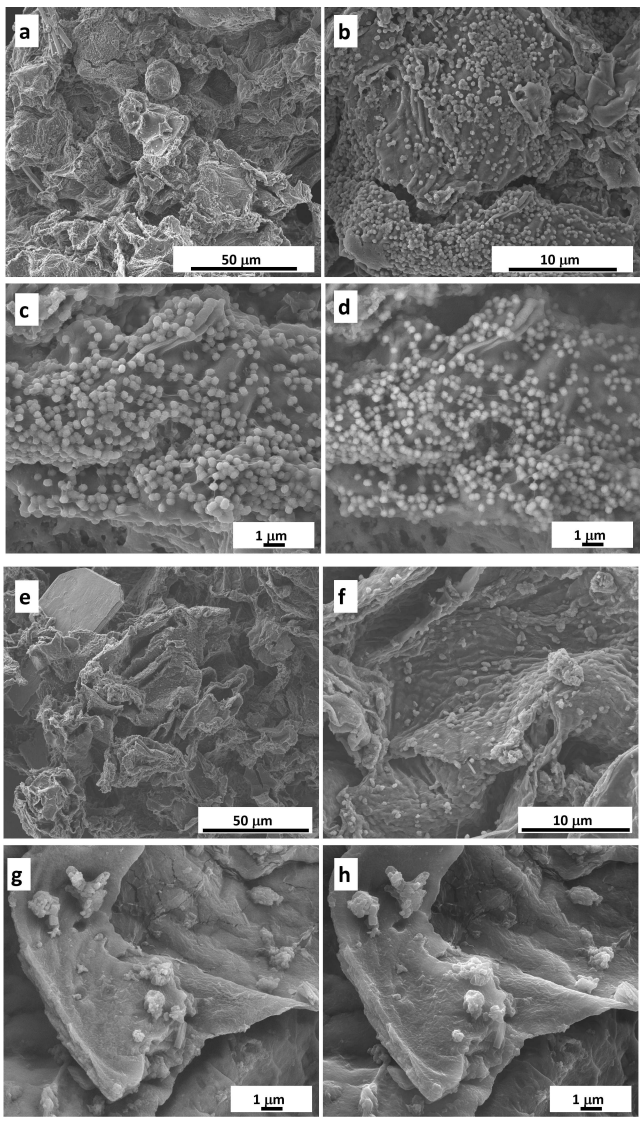

Figure 1. SEM micrographs taken with FEI Quanta FEG 250 SEM with varying magnifications for fresh Cu–O: a) 2000× and b) 10000× in SE mode at 5 kV acceleration voltages; c) 20000× in SE and d) in BSE mode at 7 kV acceleration voltage; SEM characterization of Cu–L: e) 2000× and f) 10000× in SE mode at 5 kV acceleration voltages; g) 20000× in SE and h) in BSE mode at 7 kV acceleration voltage.

The XPS analysis of the samples at the Cu2p$_{3/2}$, C1s and O1s core levels (Figure 2) provides more information on the surface chemical speciation of these samples. The survey spectra show the surface chemical composition of the samples, consisting mostly of Cu, O and C, with other impurities including N, Ca and S. The quantitative elemental analysis from the XPS data is reported in Table 1. Accordingly, the surface S and O content is higher for the Cu–L samples and this is consistent with sulphate species as seen in the Cu2p XPS spectra (Figure 2b). The parameters used for the fitting of the high-resolution core level spectra are described in the experimental section. The Cu 2p$_{3/2}$ XPS spectra of Cu–L and Cu–O were fitted using the model reported in ref. [11] and include a component at a BE of 933 eV (P2), which is slightly higher than the value reported for bulk Cu_2O or Cu metal (Cu(0) at 932.6 eV and Cu_2O at 932.4 eV).[12] Similar BE was reported for Cu/Cu_2O core-shell nanoparticles on thin C films, with a value of BE for the Cu_2O shell ranging from 932.3 eV to 933.8 eV[13] depending on the size of the metallic core and the surface Cu/C ratio: the larger the size of the metallic core and the higher the surface Cu/C ratio, the lower the BE. This phenomenology can be explained by considering that the XPS signal is dominated by the Cu/C interfaces, and thus a higher Cu abundance implies a thinner C overlayer enabling to probe a higher volume of the nanoparticle and as a consequence the BE shift to lower values approaching the value expected for bulk Cu_2O or metallic Cu. It must be pointed out that the relative composition of metallic Cu and Cu_2O cannot be determined form Cu2p XPS analysis, being the former found at only at a 0.2 eV higher BE, which is not possible to resolve with the resolution of the XPS instrument used. Despite, the nanoparticles of this work can be considered rather bulk from the XPS perspective, we can safely assume a similar situation exists here, with the P2 signal representing a Cu_2O phase covered by a C overlayer. The UV-Vis spectra reported in the Figure S2a of the supporting information confirms the presence of a metallic core in both samples, more so for Cu–O.[14]

Table 1. XPS Elemental analysis (in weight %).[a]

Sample	C	N	O	S	Cu
Cu–O	67.20	1.32	24.76	2.04	4.67
Cu–L	48.18	0.83	34.81	6.73	9.44
T–Cu–O	72.51	2.38	16.20	2.35	6.56
T–Cu–L	76.33	2.57	13.98	1.84	5.28

[a] X-ray excitation energy Al Kα (1486.6 eV) corresponding to an information depth of 5 nm at the Cu2p.[24]

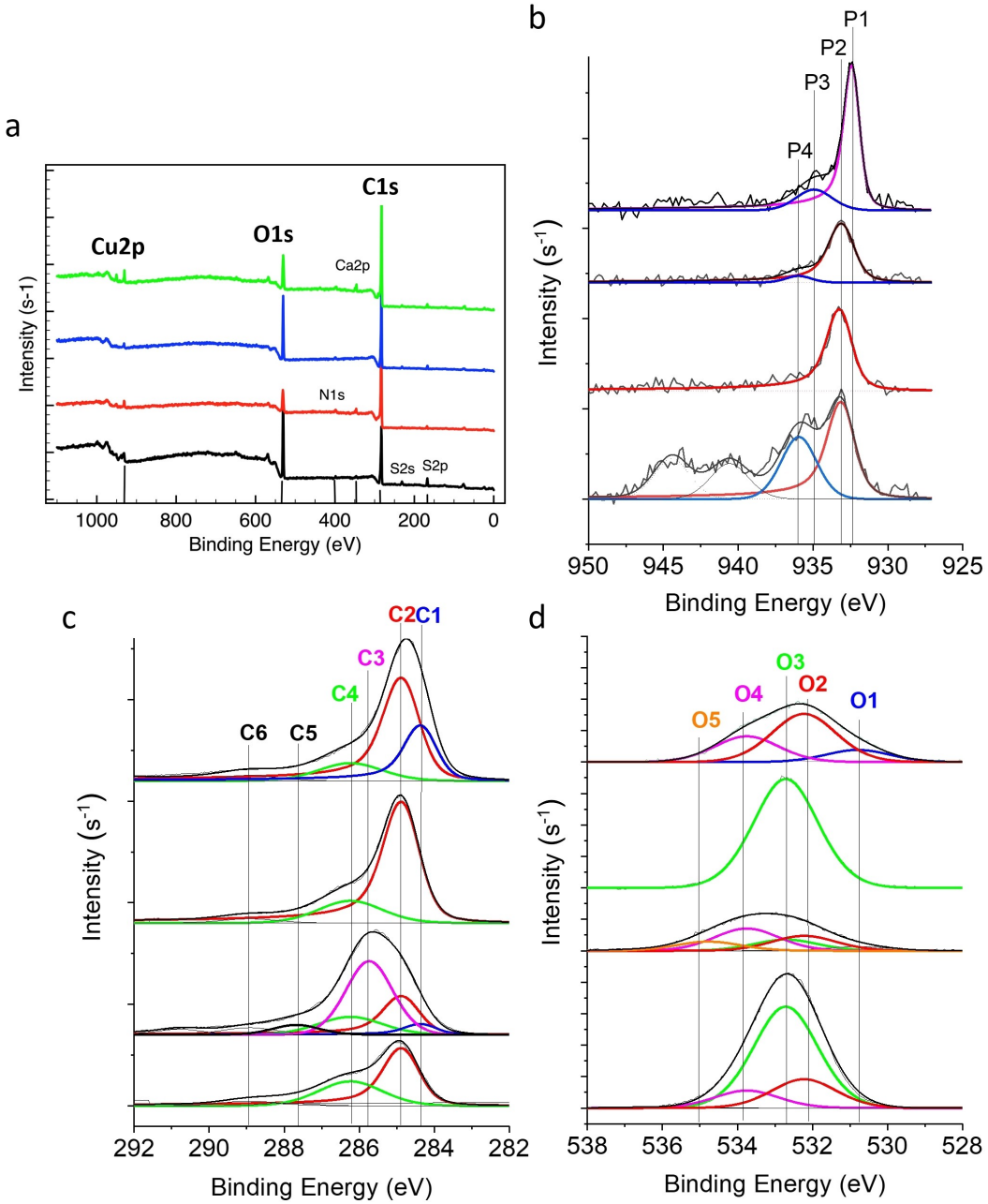

Figure 2. XPS analysis of the samples investigated using PHI VersaProbe II (Physical Electronics), equipped with an Al Kα (1486.6 eV) X-ray source. From bottom to top: Cu–L; T–Cu-L; Cu–O; T–Cu–O. a) Survey spectra; b) Cu 2p3/2; c) C1s; O1s. Spectra were calibrated with respect to the Ag 3d spectrum of a Ag foil reference. The fitting was applied consistently to each spectrum.

A component at 935.9 eV (P4) in the Cu2p spectra (Figure 2b) more abundantly on Cu–L is assigned to Cu(II) and is accompanied by satellite peaks at approximately 941 eV and 944 eV, consistent with literature.[11] We postulate that this species is related to sulphate Cu species[15] derived from the precursor used (Cu(II) aquo-sulphate complex), which remained unreduced under the synthesis conditions of Cu–L, formed as an unsupported particles precipitated during the centrifugation step. The nature of the C support in the as-synthesized materials can be evaluated at the C1s XPS (Figure 2c). By applying a fitting earlier developed in our group,[16] two main components are found, namely C2 (red component at circa 284.8 eV) and C4 (green component at 286.2 eV). An additional minor component is also found at 288.9 eV (C6 component). The samples differ in terms of C speciation as indicated by the relative ratio between C2 and C4. C2 component is attributed to the coexistence of sp^3 C–C species bound to an aromatic ring and more in general to highly disordered graphite with larger contribution from C in sp^3 bonding environment (accounts also for larger holes in basal graphitic planes);[16] its formation is consistent with the deoxygenation of aliphatic fragments of the cellulose and

lignin components of the starting peel during the hydrothermal synthesis. The C4 component is associated to C–O species such as methoxy species[11] and it is the most intense component in the C1s spectrum of cellulose.[17] Thus, it is correct to infer that in the Cu–L, some of the original peel remains unaltered after the hydrothermal synthesis. The C6 component is generally attributed to carbonates.[11] The ATR-IR spectra in Figure S2b confirm the more aliphatic and less conjugated nature of the C-backbone of the C matrix in Cu–L compared with Cu–O.

For simplicity, the O1s spectrum of Cu–O in Figure 2d was well fitted with one component at 532.7 eV (O3); however, it must be clarified that this peak should contain both contribution from the oxygen species on the Cu(I)–O particles (expected on the low BE region of the peak) and the O species on the C support. In addition to this broad component, Cu–L contains the O2 component at 532.2 eV and O4 component at 533.7 eV; the former is attributed to oxygen species in S–O or C–O species,[11,18] and the latter to more oxidised COO derived species on the support,[11] respectively, consistent with the oxidized species observed in the Cu2p and C1s XP spectra. These findings are interesting as they show that the chemical composition of the used peel plays a role in determining the chemical speciation in the sample of both the Cu nanostructures and the support (more reduced on Cu–O), which ultimately will determine the electrocatalytic properties of these materials. Intuitively we tend to attribute this phenomenon to the higher concentration of ascorbic acid in the orange peel than in the lemon peel as reported in the literature.[19] In a control study, we were able to prove the formation of Cu(I)-oxide particles from a Cu sulphate aqueous solution in the presence of ascorbic acid under the same condition of hydrothermal synthesis used here, whereas for example, phytic acid and citric acid, other chemical constituents usually abundant on the lemon peel,[19] were ineffective (not shown). However, orange peel is enriched with other antioxidants that can play a role during the synthesis. The differences in the chemical compositions of the orange and lemon peel were assessed by IR spectroscopy (Figure S3), including how they transform due to the hydrothermal treatment into the C support for the Cu nanoparticles in Cu–O and Cu–L. A more detailed discussion is presented in the supporting information. Briefly, it is possible to note (Figure S3a) that the orange peel is characterized by a more intense broad OH band and less intense C=O vibration peaks, consistent with constituents presenting more reduced alcoholic functionalities, which are essential for the antioxidant properties of organic molecules. The transformation of the orange peel (Figure S3b) includes the loss of alkane CH as well as C–O single bonds from the cellulosic component of the peel, and the formation of C=C double bonds consistent with the dehydrogenation/deoxygenation to form unsaturated conjugated C=C bonds. In contrast, the lemon peel (Figure S3c) transforms by increasing the terminal CH, including in aromatic rings, as well the C–O single bonds as a result of a dehydrogenation of the aliphatic rings of the cellulosic constituent and condensation reactions between oxygenated species, respectively. The extend of conjugation of the unsaturated C=C backbone π-system and formation of condensed ring is however more limited.

In order to test the electrocatalytic performances, the as-synthesized samples were thermally treated in Ar at 500 °C for 2 hours with the goal to enhance the graphitization of the C support, which is required for electron conduction.[20] These samples are referred herein to as T–Cu–L and T–Cu–O. The thermal treatment clearly induces structural modification, which are very different for the two samples, confirming again the important role of the chemical nature of the citrus waste used. First of all, we can see that the O content decreases for both samples, more pronounced for the lemon peel derived system due to the decomposition of the Cu sulphate species (Cu2p XPS in Figure 2b) as well as for more acidic and thus more thermolabile[21–22] oxygenated functional groups on C such as species containing C–O single bonds (Figure S2b). The N content is now very similar for both lemon and orange derived systems, whereas the Cu content apparently changes for both samples. It must be noted that XPS is a surface sensitive technique with a probing depth of approximately 5 nm in the Cu2p measurements (KE 560 eV)[16] and therefore an increase in the particle size (thus reduction of the metal dispersion) or an increase in the thickness of a C overlayer might result in the apparent reduction of the metal content.[23] This transformation can be assumed occurring for the T–Cu–L case, as will be shown later on. In contrast, the apparent increase of the metal loading in T–Cu–O can be explained by a higher weight of Cu on the overall composition due to the desorption of thermolabile species, or due to a reduction of the thickness of the surface C overlayer with no large change of the particle size distribution. We now analyse the high resolution XPS spectra.

In the case of T–Cu–L, the $Cu2p_{3/2}$ XPS spectrum shows only the P2 component, which we attributed earlier to Cu(I) species in Cu_2O. The C1s spectrum for this sample shows additional components: C1 component at 284.3 eV attributed to sp^2 graphitic carbon;[16] a dominant C3 component at 285.7 eV attributed to sp^3 C ($–CH_3$) in amorphous carbon;[11,16] C5 component at 287.7 eV due to C–O species.[11,16] As expected, this result indicates a deoxygenation/dehydrogenation of the C support, consistent with the significant reduction of the abundance of the O species shown in the O1s spectrum. The additional O5 species at circa 535 eV is generally attributed to chemisorbed water and it is commonly found on C materials especially after a thermal treatment.[21] The reduction is more effective for the T–Cu–O which is now characterized by a predominant component in the Cu $2p_{3/2}$ XPS spectrum (P1 at 932.4 eV), together with a minority of Cu(II)–OH[15] species (P3 at 934.9 eV), consistent with the appearance of O1 component in the O1s spectrum for this sample. The P1 component is 0.6 eV shifted to lower BE than the P2 component, suggesting that the shell of the nanoparticle remains a Cu_2O phase but the metallic core has grown in size upon thermal annealing.[13] The C1s spectrum for Cu–O shows a more pronounced graphitization of the carbon support (C1 component in blue).

The SEM images for the thermally treated samples (Figure 3) show to some extent sintering of the Cu particles. Nevertheless, the smaller particles are retained on the T–Cu–O indicating a great particle stabilization induced by the support. The thermally treated samples were used as electrocatalysts and tested in the electrochemical CO_2 reduction in CO_2-saturated KOH solution (0.1 M), using a custom-made three-electrode electrochemical cell previously described.[25] The data for the 2 hours tests at −1.8 V and −2 V vs Ag/AgCl are summarized in Figure 4 and Table 2. Accordingly, the CO_2 reduction products formed are formic acid (FA) and oxalic acid (OA) at both voltages and for both electrocatalysts investigated, with FA as the main product.

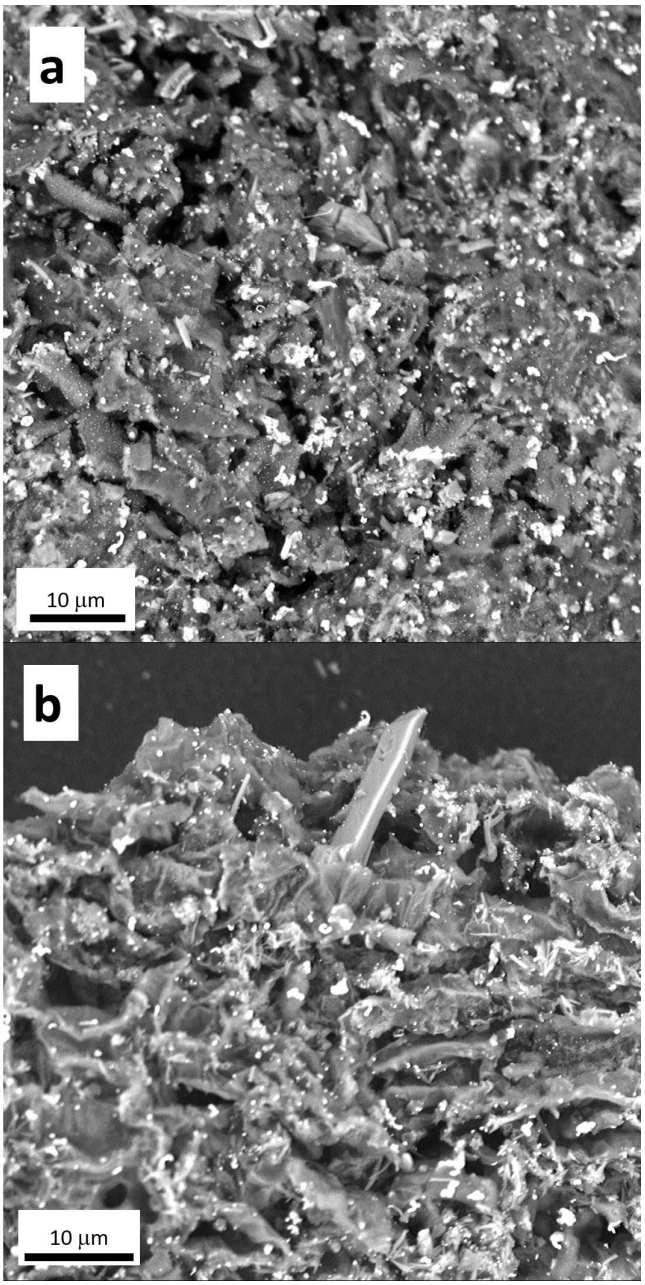

Figure 3. SEM images recorded with a Phenom ProX Desktop instrument at 10 kV acceleration voltage in BSE mode: a) T–Cu–O at ×4000 magnification; b) T–Cu–L at ×4500 magnification.

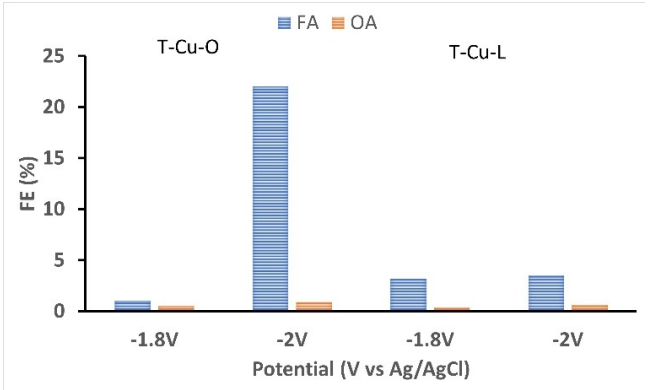

Figure 4. Faradaic efficiency (EF) to formic acid (FA) and Oxalic acid (OA) of the T–Cu–O and T–Cu–L electrodes, after 2 hours of testing.

Table 2. Summary of Faraday efficiency (FE).[a]

Sample	$FE_{Formic\ Acid}$ [%]	$FE_{Oxalic\ Acid}$ [%]	Voltage [V]
T–Cu–O	1.0	0.5	−1.8
T–Cu–L	3.2	0.4	−1.8
T–Cu–O	22.0	1.0	−2.0
T–Cu–L	3.5	0.6	−2.0

[a] After 2 h testing in CO_2 sat. KOH.

The main product detected is H_2 via the parasitic hydrogen evolution reaction (HER). Moreover, traces of methane and ethylene were observed at all the potential investigated. It can be observed that the performances of T–Cu-L electrode are not changing significantly at the two voltages investigated with a Faraday efficiency (FE) to FA slightly below 5%. In contrast, the performances are significantly improved for the T–Cu–O electrode when the voltage is lowered to −2 V vs. Ag/AgCl with FE to FA reaching a 22%.

We also observed an increased stability of T–Cu–O which leads to the formation of formic acid with faraday efficiency approaching 35% after 3 h, whereas the T–Cu–L is unstable after 3 h and its performance deteriorates drastically. This suggests that improvements of the long-term stability of the electrode should aim at strengthening the interaction between the catalyst and the gas diffusion layer used as the current collector.

The formation of FA is of high commercial interest, due to its potential use as a safe H_2-vector molecule.[26] Over pure Cu electrocatalyst, FA is generally produced in $KHCO_3$ electrolytes at a lower overpotential, generally in the range of 1.1–1.5 V vs. Ag/AgCl, with a FE ranging between 5–40%, which decreases substantially at more negative voltages.[27] In a systematic study on the impact of the electrolyte, KOH was found to produce the lowest amount of formic acid owing to its high pH which is found to be detrimental for this reaction.[28] In this study, the pH effect, the incomplete graphitization (Figure 2b) or the Cu surface decoration with a C overlayer (Figure 1 c,d) might lead to a slightly higher overpotential for the formation

of FA if compared to pure Cu systems in $KHCO_3$, though we achieve similar efficiencies.[27]

To explore further the impact of the thermal annealing of the carbon support, we performed additional experiments in which the as-synthesized samples were thermally treated in Ar at 800 °C (T800-Cu–O and T800-Cu–L). The results of the electrocatalytic tests are reported in Table 3. Accordingly, we can see a deterioration of the CO_2RR activity for T800-Cu–O and T800-Cu–L, with the latter one being the least selective sample towards CO_2-reduction products. The XPS spectra for these samples are reported in Figure S4 and Tables S1 and S2. The analysis of the C1s confirm the effective enhancement of the graphitization degree of the C support more pronounced for T800-Cu–O than T800-Cu–L. However, the Cu speciation also changes with a treatment at such a high temperature with a significant increase of the abundance of Cu(II) oxy-hydroxide species. The presence of these species can be explained by considering that they form upon exposure of the samples to the environment after the thermal treatment and indicate an exposed Cu surface as opposed to the T–Cu–O and T–Cu–L samples in which the Cu nanostructures are to some extent protected by a C overlayer.

The CO_2RR reactivity data of T800-Cu–O and T800-Cu–L suggest for a role of the carbon support more complex than simply an electrical conductor medium where the degree of graphitization is the primary structural characteristic to maximize. In fact, the optimal balance between the dispersion and stabilization of the Cu particles, the population of CO_2-chemisorption sites, the control of Cu exposure to H^+ and the support electron conduction must be achieved for enhanced CO_2RR performances. By operando spectroscopic techniques, it is consistently found that Cu under CO_2RR is predominantly in a metallic state.[29] In this work, the excessive exposure of Cu is demonstrated to be detrimental for CO_2 reduction whilst favoring the HER, suggesting that the carbon overlayer has an important role in controlling the selectivity. Indeed, the role of the C overlayer in controlling the selectivity of metal NPs is well-known in heterogeneous catalysis.[30]

Nevertheless, these results confirm the beneficial effect of the orange peel constituents, which manifests itself during the synthesis of the electrocatalyst with consequences on the CO_2RR performances. On Cu–O, we have achieved a good control of particles size as well as a better stabilization of the particles on a resulting C support with a more favorable structure for application in electrocatalysis. Good Cu dispersion is required for higher CO_2RR products productivity; the carbon support should be sufficiently functionalized to stabilize the particles but also sufficiently graphitic to allow electron conduction. Substitutional heteroatoms on the C matrix such as N, S and O species with basic character are generally beneficial for this purpose especially when metal is immobilized by a wet impregnation method.[31] On T–Cu–L, the N and O abundances are very similar to T–Cu–O and therefore these species seem of secondary important for explaining the performances observed. Under CO_2RR, due to the incomplete Cu reduction as well as a dominant polymeric nature of the C support, T–Cu–L will undergo a structural transformation that accounts for the observed deterioration of the electrode. Increasing the temperature of the thermal annealing from 500 °C to 800 °C did not result in an improvement of the performances, although one cannot exclude that the thermal annealing in inert and the procedure to stabilize the catalyst on the gas diffusion layer could be further optimized. This is however beyond the scope of this contribution. In the case of T–Cu–O we observed the best balance of these physiochemical properties of the carbon support and the electronic structure and dispersion of the Cu active phase. We should point out that Cu(I) species are indeed needed for CO_2 activation.[32]

The different chemical speciation between the orange peel derived and lemon peel derives systems is an interesting result showing an opportunity for application-oriented tunability of the synthesis and the use of biomasses waste. The comparative analysis of the original peels and after the Cu NPs immobilization has indicated a small difference in the chemical speciation of the peels, with the orange peel being more hydrophilic and presenting more and stronger reducing functionalities. These differences lead to a pronounced difference in the nature of the species on the C support, with a deoxygenation/dehydrogenation of the cellulose/lignin structural units for Cu–L, which progress further on Cu–O towards condensation of aromatic rings and extended π-conjugation. Following the Cu immobilisation, a thermal annealing of the sample can further favour the ring condensation process and deoxygenation of the C support, at a lower temperature for the orange peel derived samples than for the lemon peel (see comparative analysis of the distribution of C species on the samples at the different synthesis conditions in Figure S4). However, the post-synthesis thermal treatments generally suffer from a poor control of the particle size whereas the use of capping agents in wet chemistry to prevent particles overgrowth gives generally better results.[23,31] Considering a correlation between the more hydrophilic nature of the orange peel (more extended H-bond-OH network in Figure S3a) and the very good control of Cu particle size obtained on this system compared with the lemon peel system, one could postulate that the orange peel releases some of the water soluble, low molecular weight compounds with reducing properties for Cu solvated cations, including ascorbic acid. Our hypothesis was indeed whether these constituents of the peels could be utilized directly in the reduction of aqueous Cu species in a one pot synthesis without any additional

Table 3. Faraday efficiency (FE) for post-treated samples at different temperature.[a]

Sample	$FE_{Formic\ Acid}$ [%]	$FE_{Oxalic\ Acid}$ [%]	Av. Current [A]
T–Cu–O	5.3	1.4	$-3.43\cdot10^{-2}$
T–Cu–L	3.6	1.3	$-3.46\cdot10^{-2}$
T800-Cu–O	3.0	1.0	$-2.64\cdot10^{-2}$
T800-Cu–L	2.8	0.9	$-3.62\cdot10^{-2}$

[a] Summary of CO2RR FE after 1 h testing in CO_2 sat. KOH at −2 V vs Ag/AgCl. H_2 is the main product with a FE coinciding with the theoretical value.

additives. To rationalize this finding, a preliminary study by liquid chromatography mass spectrometry (LC-MS) of the aqueous supernatant after the hydrothermal treatment of the peels with or without Cu sulphate indicates not only minor differences in terms of the quantity of ascorbic acid present, which we suggested initially as the primary reducing agent, but also a different composition of other naturally occurring antioxidant constituents (catechins) between the orange peel and the lemon peel. Particularly a component associated to epicatechin[33] is present only in the aqueous supernatant of the orange peel and it is consumed during the hydrothermal synthesis of the Cu NPs (basically in the supernatant when Cu sulphate is also added to the initial suspension), indicating a potential beneficial role of these in the control of the particle size as well as the deoxygenation of the C matrix by these compounds. It means that these antioxidants are released in solution first to reduce the Cu(II) aquo-sulphate-complex to from nanoparticles and then adsorb onto them preventing further growth. The nanoparticles are then deposited on the insoluble part of the peel and preserved upon thermal annealing. In contrast, Cu(II) aquo-sulphate-species, which were not reduced by the naturally occurring antioxidants, adsorb on the cellulosic insoluble component of the peel as atomically dispersed species and act as nucleation center to produce larger sulphate particles during the hydrothermal treatment and upon centrifugation.

Conclusions

Herein we developed successfully a one-pot synthesis of Cu electrocatalyst from biomass derived precursors active in the electroreduction of CO_2. This contribution shows the importance of the nano structural characteristics of the electrode in improving the performances of the electrocatalysts with opportunity for tunability even starting from biomass derived C precursors with intrinsically a very complex chemical composition. In fact, we have identified the multifactorial role of the carbon support in electrocatalysis (electrical conductor, templating role in the nanoparticles formation, stabilization and controlled metal exposure during electrocatalysis) and the unique opportunity offered by functionally complex chemical waste such as orange peel to realize this. The relevance of this contribution stems on the fact that it demonstrates the viability of a direct utilization of the citrus waste to produce useful materials in a green fashion without the addition of any templating agent as well as reducing agent; it provides a rational strategy for tailored synthesis and thus, a framework for further exploring effectively this carbon source. We showed that waste from orange peel are a suitable alternative for the largescale production of C-supported Cu nanoparticles, and while our immediate focus was on the CO_2 reduction reaction, our findings can be generally applied to the preparation of orange peel derived C-supported metal electrocatalysts for other electrocatalytic reactions of relevance in storage and energy conversion as well as for any applications in which a homogeneous Cu distribution is required.

Experimental Section

Synthesis of Cu catalyst samples: In our synthetic protocol, 3 g of $CuSO_4$ (anhydrous powder, 99.99% purity from Sigma Aldrich) was dissolved in 30 mL of distilled water at 50 °C for 10 minutes. Two commercial citrus peels from Nutripowder were used, namely the orange peel and the lemon peel. 0.65 g of finely grinded citrus peel powder, either from lemon or orange, was suspended in 4 mL of the $CuSO_4$ solution and diluted to 8 mL with distilled water in a 10 mL microwave tube, thus irradiated at 68 °C for 11 minutes using a CEM Discover Microwave Reactor. The suspension was allowed to cool for 2 minutes and centrifuged at 1500 rpm for 8 minutes. The solid material was washed with distilled water and ethanol, vacuum filtered and used for further analyses and testing. These are here refereed to as Cu–O and Cu–L.

Electrode preparation: The as prepared catalysts were thermally annealed in Ar for 2 h at 500 °C with a ramp of 5 °C/min, (T–Cu–O and T–Cu–L) and at 800 °C (T800-Cu–O and T-800-Cu–L). An ink of the thermally treated electrocatalyst was prepared by mixing together 8 mg of catalyst (equivalent to 0.5 mg/cm^2), 10 μl of Nafion (Aldrich, 10 wt%), and 1.1 ml of absolute ethanol anhydrous (Carlo Erba) and sonicated for 2 hours. Then the so prepared ink was deposited on SIGRACET GDL 28 BC (surface 16 cm^2) by spray coating.

Electrocatalytic tests: The ink containing the catalyst was first deposited on a graphitic gas diffusion layer (GDL) or the glassy carbon disk and then used as a working electrode. Stability test were performed in 0.1 M KOH on both a glassy carbon working electrode and a GDL working electrode (WE), for comparison, using an electrochemical cell configuration as described in ref. [25]. In this cell, a Ag/AgCl electrode was the reference electrode and a platinum wire was the counter electrode. After flushing the electrolyte with N_2, a series of voltammetric cycles were performed in CO_2-saturated 0.1 M KOH solution, showing redox waves typical of Cu. This confirms that despite the apparent encapsulation of the Cu nanoparticles by the carbon overlayer, the CV enables to expose active Cu surface. The chronoamperometric electrochemical experiments were performed on the GDL-based working electrode at two constant applied voltages, first at −1.8 and then at −2 V vs. Ag/AgCl at 25 °C, by monitoring the current density via a potentiostat (Amel Model 2551) for 1 hour, 2 hours and 3 hours. The products were analysed by ion chromatography (Metrohm), using 0.5 mM H_2SO_4 as mobile phase, with a flow of 0.5 mL/min, at an average pressure of 5 MPa. Between each step, CV cycles were performed to evaluate changes in the redox response. A blank experiment was also performed using a Nafion/ethanol-impregnated GDL (no catalyst) in CO_2-saturated 0.1 M KOH, the absence of CO_2 reduction products confirms that the catalysts are the active materials for the CO_2RR.

The Faraday efficiency is calculated according to the following Equation (1):

$$FE = (\alpha \cdot n \cdot F)/Q \quad (1)$$

where α is the number of electrons transferred (e.g., $\alpha = 2$ for CO_2 reduction to HCOOH); n is the number of moles of the product yielded; F is the Faraday's constant (96485 C mol^{-1}); Q is the average charge passed.

Characterization

X-ray fluorescence analysis of the samples was performed using a Thermo Fisher Niton XL3 instrument. A FEI Quanta FEG 250 SEM

Table 4. Summary of XPS Fitting.[a]

Cu2p (BE)[b]	P1 (932.4)	P2 (933.1)	P3 (934.9)	P4 (935.9)	Sat 1 (941)	Sat 2 (944)
LS/ FWHM[c]	DS(0.1,299)/ 1.2	DS(0.1,299)/ 2-2.2	GL(30)/ 2.8	GL(30)/ 2.8	GL(30)/ 3	GL(30)/ 3
C1 s (BE)[b]	C1 (284.3)	C2 (285.8)	C3 (285.7)	C4 (286.2)	C5 (287.7)	C6 (288.9)
LS/ FWHM[c]	DS(0.1,450)/ 1	DS(0.1,450)/ 1.1	GL(30)/ 1.5	GL(30)/ 2	GL(30)/ 1.5	GL(30)/ 1.5
O1 s (BE)[b]	O1 (530.8)	O2 (532.2)	O3 (532.7)	O4 (533.7)	O5 (534.7)	
LS/ FWHM[c]	GL(30)/ 2	GL(30)/ 2	GL(30)/ 2	GL(30)/ 2	GL(30)/ 2	

[a] Peak fitting was performed using CASAXPS software after a Tougaard background subtraction. [b] BE: Binding energy (in eV). [c] FWHM:Full width at half maximum (in eV).

was used for morphological characterization of the fresh samples, whereas the thermally treated samples were characterized using a Phenom ProX Desktop instrument. The measurements were performed in secondary electron mode and backscattered at an acceleration voltage as indicated in each case.

XPS analysis was performed directly on the samples in powder form using PHI VersaProbe II (Physical Electronics), equipped with an Al Kα (1486.6 eV) X-ray source. The parameters used for the fitting of the XPS peaks are summarized in Table 4.

Acknowledgements

R. A. and T. M wish to acknowledge Amy Evans and Lee Harman at the University of Salford for performing XRF analysis and for support with LC-MS analysis, respectively.

Conflict of Interest

The authors declare no conflict of interest.

Keywords: Biomass upgrade · Carbon · CO_2RR · Formic acid · microwave assisted hydrothermal synthesis

[1] a) A. Iemhoff, M. Vennewald, J. Artz, C. Mebrahtu, A. Meledin, T. E. Weirich, *ChemCatChem* **2022**, *14*, e202200179; b) R. Arrigo, M. E. Schuster, S. Abate, G. Giorgianni, G. Centi, S. Perathoner, *ACS Catal.* **2016**, *6*, 6959–6966; c) A. Villa, D. Wang, P. Spontoni, R. Arrigo, D. Su, L. Prati, *Catal. Today* **2010**, *157*, 89–93; d) S. S. Chen, J. M. Carraher, G. Tuci, A. Rossin, C. A. Raman, L. Luconi, D. C. W. Tsang, G. Giambastiani, J.-P. Tessonnier, *ACS Sustainable Chem. Eng.* **2019**, *7*, 16959.

[2] a) R. Arrigo, R. Blume, V. Streibel, C. Genovese, A. Roldan, M. E. Schuster, C. Ampelli, S. Perathoner, J. J. Velasco Vélez, M. Hävecker, A. Knop-Gericke, R. Schlögl, G. Centi, *ACS Catal.* **2022**, *12*, 411–430; b) P. Tang, H. J. Lee, K. Hurlbutt, P.-Y. Huang, S. Narayanan, C. Wang, D. Gianolio, R. Arrigo, J. Chen, J. H. Warner, M. Pasta, *ACS Catal.* **2022**, *12*, 3173–3180; c) J. P. Victoria Tafoya, S. Doszczeczko, M. M. Titirici, A. B. Jorge Sobrido, *Int. J. Hydrogen Energy* **2022**, *47*, 5462–5473.

[3] a) M. W. Thielke, G. Tian, A. J. Sobrido, *J. Phys. Mater.* **2022**, *2*, 024004–024004; b) H. Au, H. Alptekin, A. C. S. Jensen, E. Olsson, C. A. O'Keefe, T. Smith, M. Crespo-Ribadeneyra, T. F. Headen, C. P. Grey, Q. Cai, A. J. Drewb, M.-M. Titirici, *Energy Environ. Sci.* **2020**, *13*, 3469–3479.

[4] M.-M. Titirici, R. J. White, N. Brun, V. L. Budarin, D. S. Su, F. del Monte, J. H. Clark, M. J. MacLachlang, *Chem. Soc. Rev.* **2015**, *44*, 250–290.

[5] M. Raimondo, F. Caracciolo, L. Cembalo, G. Chinnici, B. Pecorino, M. D'Amico, *Sustainability* **2018**, *10*, 4821.

[6] J. N. Tiwari, N. K. Dang, S. Sultan, P. Thangavel, H. Y. Jeong, K. S. Kim, *Nat. Sustain.* **2020**, *3*, 556–563.

[7] A. R. Galletti, C. Antonetti, V. De Luise, D. Licursi, N. Nassi, *BioResources* **2012**, *7*, 1824–1835.

[8] https://www.grandviewresearch.com/industry-analysis/citrus-extract-market.

[9] K. Sharma, N. Mahato, M. H. Choo, Y. R. Lee, *Nutrition* **2017**, *34*, 29–46.

[10] a) A. Loiudice, P. Lobaccaro, E. A. Kamali, T. Thao, B. H. Huang, J. W. Ager, *Angew. Chem. Int. Ed.* **2016**, *55*, 5789–5792; *Angew. Chem.* **2016**, *128*, 5883–5886; b) B. C. Marepally, C. Ampelli, C. Genovese, F. Tavella, E. A. Quadrelli, S. Perathoner, G. Centi, *J. CO2 Util.* **2020**, *35*, 194–204.

[11] a) R. Arrigo, R. Blume, A. Ian Large, J. Jesus Velasco-Vélez, M. Hävecker, A. Knop-Gericke, G. Held, *Faraday Discuss.* **2022**, *236*, 126–140, Advance Article; b) P. Jiang, D. Prendergast, F. Borondics, S. Porsgaard, L. Giovanetti, E. Pach, J. Newberg, H. Bluhm, F. Besenbacher, M. Salmeron, *J. Chem. Phys.* **2013**, *138*, 024704.

[12] B.-H. Liu, M. Huber, M. A. van Spronsen, M. Salmeron, H. Bluhm, *Appl. Surf. Sci.* **2022**, *583*, 152438.

[13] T. Ghodselahi, M. A. Vesaghi, A. Shafiekhani, A. Baghizadeh, M. Lameii, *Appl. Surf. Sci.* **2008**, *255*, 2730–2734.

[14] E. Cottancin, G. Celep, J. Lermé, M. Pellarin, J. R. Huntzinger, J. L. Vialle, M. Broyer, *Theor. Chem. Acc.* **2006**, *116*, 514–523.

[15] M. C. Biesinger, *Surf. Interface Anal.* **2017**, *49*, 1325–1334.

[16] R. Arrigo, R. Blume, V. Streibel, C. Genovese, A. Roldan, M. E. Schuster, C. Ampelli, S. Perathoner, J. J. Velasco Vélez, M. Hävecker, A. Knop-Gericke, R. Schlögl, G. Centi, *ACS Catal.* **2022**, *12*, 411–430.

[17] V. Kuzmenko, N. Wanga, M. Haquea, O. Nabokac, M. Flygared, K. Svenssond, P. Gatenholmbe, J. Liua, P. Enoksson, *RSC Adv.* **2017**, *7*, 45968–45977.

[18] M. Wahlqvist, A. Shchukarev, *J. El. Spec. Rel. Phen.* **2007**, *156–158*, 310–314.

[19] K. A. Elkhatim, R. A. A. Elagib, A. B. Hassan, *Food Sci. Nutr.* **2018**, *6*, 1214–1219.

[20] L. Gai, J. Li, Q. Wang, R. Tian, K. Li, *J. Environ. Chem. Eng.* **2021**, *9*, 106678.

[21] R. Arrigo, M. Hävecker, S. Wrabetz, R. Blume, M. Lerch, J. McGregor, E. P. J. Parrott, J. A. Zeitler, L. F. Gladden, A. Knop-Gericke, R. Schlögl, D. S. Su, *J. Am. Chem. Soc.* **2010**, *132*, 9616–9630.

[22] K. F. Ortega, R. Arrigo, B. Frank, R. Schlögl, A. Trunschke, *Chem. Mater.* **2018**, *28*, 6826–6839.

[23] R. Arrigo, S. Gallarati, M. E. Schuster, J. M. Seymour, D. Gianolio, I. da Silva, J. Callison, H. Feng, J. E. Proctor, P. Ferrer, F. Venturini, D. Grinter, G. Held, *ChemCatChem* **2020**, *12*, 1491–1503.

[24] S. Tanuma, C. J. Powell, D. R. Penn, *Surf. Interface Anal.* **1994**, *21*, 165–176.

[25] F. P. Abramo, F. De Luca, R. Passalacqua, G. Centi, G. Giorgianni, S. Perathoner, S. Abate, *J. Energy Chem.* **2022**, *68*, 669–678.

[26] a) X. Lu, D. Y. C. Leung, H. Wang, M. K. H. Leung, J. Xuan, *ChemElectroChem* **2014**, *1*, 836–849; b) A. S. Agarwal, Y. Zhai, D. Hill, N. Sridha, *ChemSusChem* **2011**, *4*, 1301–1310.

[27] a) D. Ren, Y. Deng, A. D. Handoko, C. S. Chen, S. Malkhandi, B. S. Yeo, *ACS Catal.* **2015**, *5*, 2814–2821; b) N.-T. Suen, Z.-R. Kong, C.-S. Hsu, H.-C. Chen, C.-W. Tung, Y.-R. Lu, C.-L. Dong, C.-C. Shen, J.-C. Chung, H.

Ming Chen, *ACS Catal.* **2019**, *9*, 5217–5222; c) A. Dutta, M. Rahaman, M. M. Zanetti, P. Broekmann, *ACS Catal.* **2017**, *7*, 5431–5437.
[28] H.-Y. Kim, I. Choi, S. H. Ahn, S. J. Hwang, S. J. Yoo, J. Han, J. Kim, H. Park, J. H. Jang, S.-K. Kim, *Int. J. Hydrogen Energy* **2014**, *39*, 16506–16512.
[29] R. Arrigo, *Curr. Opin. Green Sustain. Chem.* **2022**, *34*, 10060.
[30] a) R. Arrigo, M. E. Schuster, S. Abate, G. Giorgianni, G. Centi, S. Perathoner, *ACS Catal.* **2016**, *6*, 6959–6966; b) R. Arrigo, S. Wrabetz, M. E. Schuster, D. Wang, A. Villa, D. Rosenthal, *Phys. Chem. Chem. Phys.* **2012**, *14*, 10523–10532.
[31] a) R. Arrigo, M. E. Schuster, *Catalysts* **2019**, *9*, 303; b) A. I. Large, S. Wahl, S. Abate, I. da Silva, J. J. Delgado Jaen, N. Pinna, G. Held, R. Arrigo, *Catalysts* **2020**, *10*, 1289.
[32] a) J. J. Velasco-Vélez, C. H. Chuang, D. Gao, Q. Zhu, D. Ivanov, H. S. Jeon, R. Arrigo, R. V. Mom, E. Stotz, H. L. Wu, T. E. Jones, B. Roldan Cuenya, A. Knop-Gericke, R. Schlögl, *ACS Catal.* **2021**, *10*, 11510–11518; b) J. J. Velasco-Velez, R. V. Mom, L. E. Sandoval-Diaz, L. J. Falling, C. H. Chuang, D. Gao, D. Gao, T. E. Jones, Q. Zhu, Q. Zhu, R. Arrigo, B. Roldan Cuenya, A. Knop-Gericke, A. Knop-Gericke, T. Lunkenbein, R. Schlögl, R. Schlögl, *ACS Energy Lett.* **2021**, *5*, 2106–2111.
[33] D. Escobar-Avello, J. Lozano-Castellon, C. Mardones, A. J. Perez, V. Saez, S. Riquelme, D. von Baer, A. Vallverdú-Queralt, *Molecules* **2019**, *24*, 3763.

Manuscript received: August 9, 2022
Revised manuscript received: November 14, 2022
Version of record online: January 9, 2023